Metabolomics
DOI 10.1007/s11306-011-0328-x

ORIGINAL ARTICLE

Cyclin-dependent kinases 4 and 6 control tumor progression and direct glucose oxidation in the pentose cycle

Miriam Zanuy · Antonio Ramos-Montoya · Oscar Villacañas · Nuria Canela · Anibal Miranda · Esther Aguilar · Neus Agell · Oriol Bachs · Jaime Rubio-Martinez · Maria Dolors Pujol · Wai-Nang P. Lee · Silvia Marin · Marta Cascante

Received: 21 February 2011 / Accepted: 22 June 2011

Abstract Cyclin-dependent kinases CDK4 and CDK6 are essential for the control of the cell cycle through the G_1 phase. Aberrant expression of CDK4 and CDK6 is a hallmark of cancer, which would suggest that CDK4 and CDK6 are attractive targets for cancer therapy. Herein, we report that calcein AM is a potent specific inhibitor of CDK4 and CDK6 in HCT116 human colon adenocarcinoma cells, inhibiting retinoblastoma protein (pRb) phosphorylation and inducing cell cycle arrest in the G_1 phase. The metabolic effects of calcein AM (the calcein acetoxymethyl-ester) on HCT116 cells were also evaluated and the flux between the oxidative and non-oxidative branches of the pentose phosphate pathway was significantly altered. To elucidate whether these metabolic changes were due to the inhibition of CDK4 and CDK6, we also characterized the metabolic profile of a CDK4, CDK6 and CDK2 triple knockout of mouse embryonic fibroblasts. The results show that the metabolic profile associated with the depletion of CDK4, CDK6 and CDK2 coincides with the metabolic changes induced by calcein AM on HCT116 cells, thus confirming that the inhibition of CDK4 and CDK6 disrupts the balance between the oxidative and non-oxidative branches of the pentose phosphate pathway. Taken together, these results indicate that low doses of calcein can halt cell division and kill tumor cells. Thus, selective inhibition of CDK4 and CDK6 may be of greater pharmacological interest, since

Miriam Zanuy and Antonio Ramos-Montoya contributed equally to this work.

Electronic supplementary material The online version of this article (doi:10.1007/s11306-011-0328-x) contains supplementary material, which is available to authorized users.

M. Zanuy · A. Ramos-Montoya · A. Miranda · E. Aguilar · S. Marin · M. Cascante (✉)
Department of Biochemistry and Molecular Biology, Faculty of Biology (Edifici Nou), University of Barcelona, Av. Diagonal 645, 08028 Barcelona, Spain
e-mail: martacascante@ub.edu

M. Zanuy · A. Ramos-Montoya · A. Miranda · E. Aguilar · S. Marin · M. Cascante
Institute of Biomedicine of the Universitat de Barcelona (IBUB) and CSIC Associated Unit, Barcelona, Spain

O. Villacañas · J. Rubio-Martinez
Department of Physical Chemistry, Institut de Recerca en Química Teòrica i Computacional (IQTCUB), Universitat de Barcelona, Martí i Franqués 1, 08028 Barcelona, Spain

N. Canela · N. Agell · O. Bachs
Department of Cell Biology, Immunology and Neurosciencies, Institut d'Investigacions Biomèdiques August Pi i Sunyer (IDIBAPS), Faculty of Medicine, Universitat de Barcelona, Casanova 143, 08036 Barcelona, Spain

M. D. Pujol
Department of Pharmacology and Therapeutic Chemistry, CSIC Associated Unit, Faculty of Pharmacy, Universitat de Barcelona, Joan XXIII, s/n, 08028 Barcelona, Spain

W.-N. P. Lee
Department of Pediatrics, Los Angeles Biomedical Research Institute at the Harbor-UCLA Medical Center, RB1, 1124 West Carson Street, Torrance, CA 90502, USA

Present Address:
A. Ramos-Montoya
Uro-Oncology Research Group, Cancer Research UK Cambridge Research Institute, Li Ka Shing Centre, Robinson Way, Cambridge CB2 0RE, UK

Present Address:
O. Villacañas
Intelligent Pharma S.L, C/Baldiri Reixac 4, 08028 Barcelona, Spain

Journal : Large 11306 | Dispatch : 27-6-2011 | Pages : 11
Article No. : 328 | ☐ LE | ☐ TYPESET
MS Code : MEBO-474 | ☑ CP | ☑ DISK

inhibitors of these kinases affect both cell cycle progression and the robust metabolic profile of tumors.

Keywords Cyclin dependent kinases · CDK-inhibitor · Tracer-based metabolomics · Pentose phosphate pathway · Phase plane analysis

Abbreviations

Calcein AM	Calcein acetoxymethyl-ester
CDK	Cyclin dependent kinase
DMEM	Dulbecco's modified eagle medium
FCS	Fetal calf serum
Ct MEF	Mouse embryonic fibroblast
PBS	Phosphate buffer saline
PPP	Pentose phosphate pathway
pRb	Retinoblastoma protein
TKO MEF	Mouse embryonic fibroblast knockout for CDK4, CDK6 and CDK2

1 Introduction

Typical proliferation of eukaryotic cells involves an orderly progression through four distinct phases of the cell cycle: G_1, S, G_2, and M (Malumbres and Barbacid 2001; Sherr 1996). The first step of the G_1/S transition of the cell cycle is regulated by cyclin-dependent kinases (CDKs: EC 2.7.11.22), CDK4 and CDK6 and their inhibitors, $p16^{INK4a}$ and $p15^{INK4b}$. According to the long-prevailing model of cell cycle control in mammalian cells, cyclin D-CDK4, cyclin D-CDK6 and cyclin E-CDK2 complexes are sequentially required to promote cell cycle entrance from quiescence, progression through the G_1 phase and transition from the G_1 to the S-phase in response to mitogenic stimulation. Cell culture and biochemical studies have indicated that cyclin D-CDK4, cyclin D-CDK6 and cyclin E-CDK2 complexes are essential and rate-limiting for the phosphorylation and inactivation of the tumor suppressor retinoblastoma protein (pRb) and the subsequent induction of the E2F-dependent transcriptional program required to enter the S-phase (Lundberg and Weinberg 1998; Malumbres et al. 2004; Sherr and Roberts 2004). This step of the cell cycle is critical. If the cell passes through the restriction point (R), it becomes insensitive to extracellular stimuli and is committed to entering the S-phase. Since almost all the regulators of this cell cycle phase are mutated in cancer (Graf et al. 2009), this phase has been considered as a valid therapeutic target. Since most mutations in human cancers affect CDK4 and CDK6 or their regulators (Hall and Peters 1996), and preclinical data indicate that the inhibition of cyclin D-dependent kinase activity may have therapeutic benefits (Graf et al. 2009; Malumbres and Barbacid 2006; Shapiro 2006; Yu et al. 2006), interest in CDK4 and CDK6 as promising targets for inhibiting cell cycle progression has been generated.

Another important and critical feature of tumor cells is their metabolic adaptation, which provides them with metabolites and energy to progress through the cell cycle. This adaptation includes the phenomenon known as the "Warburg effect" (high glycolysis in the presence of oxygen) (Warburg 1956), a high glutamine uptake, the activation of biosynthetic pathways and the over-expression of some glycolytic isoenzymes (Vizán et al. 2008). In recent years, it has become accepted that the metabolic adaptation of tumor cells also involves an enhancement of pentose phosphate pathway (PPP) fluxes and a specific imbalance between its two branches in favor of the oxidative branch versus the non-oxidative branch to maintain the high proliferative rates (Kuo et al. 2000; Poulsen and Frederiksen 1981; Ramos-Montoya et al. 2006). In previous studies, we have demonstrated that this balance between the oxidative and non-oxidative branches of the PPP is necessary to maintain the metabolic efficiency of the cancer cell for growth and proliferation, and that it can be a weakness in the robust tumor metabolic adaptation (Ramos-Montoya et al. 2006). PPP is also specifically regulated during cell cycle progression in tumor cells (Vizan et al. 2009).

In the present study, we identified calcein (4′5′-bis(*N*,*N*-bis(carboxymethyl) aminomethyl) fluorescein) as a putative inhibitor of CDK4 and CDK6 that mimics the natural inhibitor $p16^{INK4a}$ in HCT116 cells, through the use of new bioinformatic tools (Villacanas et al. 2002; Villacanas and Rubio-Martinez 2006), docking procedures (Rubio-Martinez et al. 2005) and molecular assays. Moreover, we provide experimental evidence that this CDK4 and CDK6 inhibitor counteracts metabolic adaptations which are characteristic of tumor cells, and that this metabolic fingerprint coincides with that obtained from a mouse embryonic fibroblast knockout for CDK4, CDK6 and CDK2 cell line. We demonstrate not only that calcein is a promising agent that could be a key factor in the development of a new family of selective cyclin D-dependent kinase inhibitors, but also that inhibition of CDK4 and CDK6 impairs metabolic adaptations that support tumor cell cycle progression.

2 Materials and methods

2.1 Materials

Dulbecco's modified Eagle Medium (DMEM), F-12 HAM Nutrient mixture with L-glutamine, MEM-EAGLE non-essential aminoacid solution ×100, antibiotic (100 U/ml penicillin, 100 mg/ml streptomycin), Dulbecco's Phosphate buffer saline (PBS), Trypsin EDTA solution C (0.05%

Journal : Large 11306 | Dispatch : 27-6-2011 | Pages : 11
Article No. : 328 | LE | TYPESET
MS Code : MEBO-474 | CP | DISK

trypsin–0.02% EDTA), L-glutamine solution 200 mM and sodium pyruvate solution 100 mM were obtained from Biological Industries; Fetal calf serum (FCS) and Trizol were from Invitrogen; SDS was from Fluka; Coomassie blue was from Biorad; HEPES and $MgCl_2$ were from Applichem; A-Sepharose was from Pierce; the [γ-32P]ATP, 3000 Ci/mmol, 10 mCi/ml and ECL were from Amersham; histone H1 was from Boehringer Mannheim; Bradford reagent (500-0006), Acrylamide (161-0158) and peroxidase-coupled secondary antibody were from Bio-Rad Laboratories; anti-CDK6 (sc-177), anti-CDK4 (sc-260-R), anti-cyclin D3 (sc-182) and anti-p16INK4a (sc-468) were from Santa Cruz Biotechnology; anti-cyclin D1 (06-137), anti-CDK2 (06-505) and anti-cyclin B1 (05-158) were from Upstate Biotechnology; anti-actin (691001) was from MP Biomedicals; anti-phospho-Rb (Ser780) was from Cell Signaling Technology; pGST-Rb (379-928) (gift of Dr Wang, San Diego, CA, USA) fusion protein was expressed and purified following Smith and Johnson (1988) and Frangioni and Neel (1993). All other reagents were from Sigma Chemical CO.

2.2 Molecular modeling

Construction and molecular dynamics simulations of the CDK6-$p16^{INK4a}$ complex and the determination of their interactions were carried out as described Villacañas et al. 2002. All hot spots of the CDK6-$p16^{INK4a}$ interaction surface were monitored throughout the production time to obtain its pharmacophores. Catalyst (Accelrys, Inc., San Diego, CA, USA) software was then used to obtain compounds that matched the different interaction pharmacophores. Selected compounds were docked into CDK6 with an in-house program (Rubio-Martinez 2005) and, finally, a visual structure analysis was carried out to reduce the number of final modeled complexes. More details can be found in supplementary material.

2.3 Cell culture

Human colon carcinoma HCT116 cells (donated by Dr. Capellà, the Institut Català d'Oncologia, Barcelona, Spain) were grown in DMEM:HAM's F12 (1:1), supplemented with 10% heat-inactivated FCS, 2 mM glutamine, 1 mM sodium pyruvate, 1% non-essential amino acids, 50 mU/ml penicillin and 50 µg/ml streptomycin. All cell cultures were carried out at 37°C in a humidified atmosphere with 5% CO_2.

Mouse embryonic fibroblast (Ct MEF) and mouse embryonic fibroblast knockout for CDK4, CDK6 and CDK2 (TKO MEF) cell lines, obtained from Dr. Barbacid (Centro Nacional de Investigaciones Oncológicas, Madrid, Spain) (Santamaria and Ortega 2006), were grown as a monolayer culture in minimum essential medium (DMEM with L-glutamine, without glucose or sodium pyruvate) in the presence of 10% heat-inactivated FCS, 10 mM D-glucose and 0.1% streptomycin/penicillin in standard culture conditions. They were incubated at 37°C, 80% humidity, 5% CO_2, and 3% O_2. Two different clones of each were used in order to discard the effect of immortalization: Ct MEF: LD179.10.1 and LD207.3.1 and TKO MEF: LD1043.7.1 and LD1043.6.1.

2.4 Immunoprecipitation and kinase assays

For the kinase assays, immunoprecipitations were performed as described by Harlow and Lane (Harlow and Lane 1988). HCT116 cells were lysed for 30 min at 4°C in IP buffer (50 mM HEPES pH 7.5, 150 mM NaCl, 2.5 mM EGTA, 1 mM EDTA, 0.1% Tween 20, 10% glycerol, 1 mM DTT, 1 mM phenyl methyl sulfonyl fluoride, 1 µg/ml aprotinin, 10 µg/ml leupeptin, 10 mM ß-glycerophosphate, 0.1 mM Na_3VO_4 and 1 mM NaF). Lysates were sonicated twice for 10 s at 4°C and clarified by centrifugation at 10,000×*g* for 10 min. The supernatant fraction protein content was measured using the Bradford method (Bradford 1976), and 400 µg of protein from the lysates were incubated with 4 µg of antibody (CDK6, CDK4, cyclin-D1, cyclin-D3, cyclin-B1 or CDK2) or with 1 µl of normal rabbit serum or normal mouse serum (controls) O/N shaking at 4°C. Protein immunocomplexes were then incubated with 20 µl protein A-Sepharose for 1 h at 4°C, collected by centrifugation and washed four times in IP buffer and twice in kinase buffer (50 mM HEPES pH 7.4, 10 mM $MgCl_2$, 2.5 mM EGTA, 0.1 mM Na_3VO_4, 10 mM ß-glycerophosphate and 1 mM DTT). They were then incubated in kinase buffer containing 2 Ci [γ-32P]ATP and 1 µg pGST-Rb (379-928) fusion protein for CDK6 and CDK4 kinase assays, or 3 µg histone H1 for CDK1 and CDK2 kinase assays, for 30 min. at 30°C in a final volume of 30 µl. The samples were pooled and redistributed to assure equal amounts of all the reagents and immunoprecipitated CDK. Finally, the samples were boiled for 5 min and electrophoresed on SDS-polyacrylamide gels, essentially as described by Laemmli (1970), and the gels were stained with coomassie brilliant blue, dried, and exposed to X-ray films at −80°C. The intensity of radioactivity was measured with Typhoon Trio and Trio 9200 (GE Healthcare). $p21^{Kip/Cip}$ and purified $p16^{INK4a}$ were used as a positive control of inhibition.

2.5 Gel electrophoresis and immunoblotting

Cells were lysed in a buffer containing 2% SDS, 67 mM Tris–HCl pH 6.8 and 10 mM EDTA and sonicated twice for 10 s (4°C). Protein content was measured according to the Lowry procedure, using bovine serum albumin (BSA) as standard. The extracts were electrophoresed in SDS-

Journal : Large 11306 | Dispatch : 27-6-2011 | Pages : 11
Article No. : 328 | LE | TYPESET
MS Code : MEBO-474 | CP | DISK

polyacrylamide gels, essentially as described by Comin-Anduix et al. 2002 and Laemmli 1970. After electrophoresis, the proteins were transferred to Immobilon-P strips for 1.5 h at 70 V. The sheets were preincubated in TBS (20 mM Tris–HCl pH 7.5, 150 mM NaCl), 0.05% Tween 20 and 3% BSA for 1 h at room temperature and then incubated for 1 h at room temperature in TBS, 0.05% Tween 20, 3% BSA containing anti-phospho-Rb (Ser780), anti-CDK4 (sc-260), anti-CDK2 (06-505) or anti-actin (60100) antibodies. After washing in TBS, 0.05% Tween 20 (three times, 10 min each), the sheets were incubated with a peroxidase-coupled secondary antibody (1:3000 dilution) for 1 h at room temperature. After incubation, the sheets were washed twice in TBS, 0.05% Tween 20 and once in TBS. The reaction was visualized using ECL. The Image LAS-3000 Photo Version 2.0 (Fujifilm) was used to analyze the chemiluminescence.

2.6 Viability assay

The assay was performed using a variation of the method described by Mosmann (Matito et al. 2003; Mosmann 1983; Ramos-Montoya et al. 2006). Growing concentrations of the product were plated in 96-well flat-bottomed microtiter plates to a final volume of 200 µl where 1700 cells/well had been seeded 24 h before. After incubation for 72 h, MTT at a final concentration of 0.5 mg/ml was added. After 1 h of incubation, the generated *formazan* was dissolved with 100 µl of DMSO per well. The absorbance was measured on an ELISA plate reader (Merck ELISA System MIOS version 3.2., Tecan Sunrise, Tecan Group Ltd.) at 550 nm. The concentrations that caused 50% inhibition of cell viability (IC_{50}) were calculated.

2.7 Cell culture synchronization and cell cycle analysis

HCT116 cells were brought to 95% cell confluence and kept confluent for 24 h with medium containing 0.5% FCS. Cells were then seeded to 50–60% cell confluence in a medium with 10% heat-inactivated FCS. Calcein AM 2 µM was added.

In order to determine the proportion of cells in each cell cycle phase (G_1, S or G_2), cell cycle analysis was assessed with flow cytometry using a fluorescence-activated cell sorter (FACS). Approximately 500,000 cells were resuspended in 0.5 ml PBS followed by the addition of 4.5 ml 70% (v/v) ethanol (Matito et al. 2003). Cells were briefly stained in PBS containing 50 µg/ml propidium iodide, 10 µg/ml DNAse free RNAse and 0.1% Triton® X-100. FACS analysis was carried out at 488 nm in an Epics XL flow cytometer (Beckman Coulter). Data from 12,000 cells were collected and analyzed using the MultiCycle program (Phoenix Flow Systems).

2.8 Isotopologue distribution analysis

Tracer studies were carried out by incubating the cells in the presence of the corresponding incubation medium containing 10 mM glucose enriched by 50% in the tracer [1,2-$^{13}C_2$]-D-glucose. After incubation for 72 h, the cell medium was removed, thereby separating the incubation medium from the cells adhered to the dishes, and all fractions were frozen in liquid nitrogen and stored at −80°C until processing.

Mass spectral data were obtained on an HP5973 mass selective detector connected to an HP6890 gas chromatograph (HCT116 with calcein AM assays) and on a GCMS-QP2010 selective detector connected to a GC-2010 gas chromatograph from Shimadzu (Ct MEF and TKO MEF assays). The settings were as follows: GC inlet 230°C (200°C for lactate measurement), transfer line 280°C, MS source 230°C and MS Quad 150°C. An HP-5 or a DB-5MS capillary column (both: length (m), 30; internal diameter (µm), 250; film thickness (µm), 0.25) was used. Spectral data were corrected using regression analysis to extract natural ^{13}C enrichment from results (Lee et al. 1991). Measurement of ^{13}C label distribution determined the different relative distribution percentages of the isotopologues, m0 (without any ^{13}C labels), m1 (with one ^{13}C), m2 (with two ^{13}C), etc., which were reported as molar fractions. $\sum m$ is the sum of the labeled species ($\sum m = m1 + m2 + m3\ldots$) and is representative of the synthesized molecules of each metabolite. The total label enrichment $\sum mn$ is the weighted sum of the labeled species ($\sum mn = m1 \times 1 + m2 \times 2 + m3 \times 3\ldots$) and is representative of the contribution of the tracer used in the synthesis of each metabolite.

Lactate from the cell culture medium was extracted with ethyl acetate after acidification with HCl. Lactate was transformed to its propylamide-heptafluorobutyric form and the ion cluster around m/z 328 (carbons 1–3 of lactate, chemical ionization) was monitored for the detection of m1 (recycled lactate through the pentose cycle) and m2 (lactate produced by glycolysis). The relative amount of glucose that is converted indirectly to lactate through the pentose cycle, known here as pentose cycle activity, is calculated by the (m1/m2)/(3 + (m1/m2)) ratio using lactate isotopologues (Lee et al. 1998).

RNA ribose was isolated by acid hydrolysis of cellular RNA after Trizol-purification of cell extracts. Ribose isolated from RNA was transformed to its aldonitrile-acetate form using hydroxylamine in pyridine and acetic anhydride. We monitored the ion cluster around the m/z 256 (carbons 1–5 of ribose, chemical ionization) to find the molar enrichment and positional distribution of ^{13}C labels in ribose (Boros et al. 1997; Lee et al. 1998). The m2 ribose originated from [1,2-$^{13}C_2$]-glucose that is converted to ribose through transketolase enzyme reactions, whereas m1

Journal : Large 11306 Dispatch : 27-6-2011 Pages : 11
Article No. : 328 LE TYPESET
MS Code : MEBO-474 CP DISK

ribose originated from glucose metabolized by direct oxidation via the oxidative steps of the PPP. The isotopologues m3 and m4 come from the recycling of the previously labeled riboses. The oxidative versus non-oxidative ratio was measured as ox/non-ox = (m1 + m3)/(m2 + m3 + 2×m4).

2.9 Sugars-phosphate determination

Hexose, triose, pentose and fructose-1,6-bis-phosphates were determined in cell monolayers frozen in liquid nitrogen as described (Vizan et al. 2007). Frozen cells were briefly scraped off the plates and 100 mM acetic acid solution at 4°C was added. The obtained homogenates were centrifuged at 0.4×*g* for 10 min at 4°C, and the supernatants containing sugar phosphate molecules were separated and kept frozen at −80°C for the following liquid chromatography/mass spectrometry (LC–MS) analysis. Chromatography was performed using an Agilent 1100 Quaternary Pump (Agilent Technologies) equipped with a refrigerated autosampler. A Nucleodex *β*-OH high-performance liquid chromatography (HPLC) column, 200 × 4 mm i.d. (Panreac Química S.A.U.) with a binary gradient at a flow-rate of 0.75 ml/min was used. Solvent A consisted of 10 mM ammonium acetate pH 4.0. Solvent B consisted of acetonitrile. Before reaching the mass spectrometer, the flow-rate was split (1:3). To reduce the residual matrix effect reaching the mass spectrometer, a divert valve (VICI Valco Instruments) drained off the LC eluent during the time in which interference was detected in order to avoid contamination of the mass spectrometer. Identification of sugar phosphates was carried out in an API-3000 tandem mass spectrometer (Applied Biosystems). The multiple reaction monitoring (MRM) transitions were 259/97 for glucose-6-phosphate and fructose-6-phosphate (hexose phosphates), 199/97 for glyceraldehyde-3-phosphate and dihydroxyacetone phosphate (triose phosphates), 339/97 for fructose-1,6-bisphosphate and 229/97 for ribose-5-phosphate and xylulose-5-phosphate (pentose phosphates).

2.10 Data analysis and statistical methods

In vitro experiments were carried out using three cultures each time for each treatment regimen and then repeated twice. Mass spectral analyses were carried out by three independent automatic injections of 1 µl of each sample by means of the automatic sampler and accepted only if the sample standard deviation was less than 1% of the normalized peak intensity. Statistical analyses were performed using the parametric unpaired, two-tailed independent sample *t* test with 95, 99, and 99.9% confidence intervals, and $P < 0.05$, $P < 0.01$, and $P < 0.001$ were considered, respectively, to indicate significant differences in glucose carbon metabolism.

3 Results

3.1 Selection of a better CDK4 and CDK6 inhibitor

Results from CDK6-p16^{INK4a} complex dynamics were used to model the interaction pattern of the putative inhibitors. The ACD 3D database (available chemical database 3D) was screened for commercial compounds that matched our query. After docking procedures, eight compounds were selected for further experimental kinase assays, with calcein being the most active (Figure SM1, Supplementary Material).

3.2 Calcein selectively inhibits CDK4 and CDK6 activities, disrupting cell growth, pRb and cell cycle

To investigate whether calcein selectively inhibits CDK4 and CDK6 activities, immunoprecipitations were performed, followed by kinase assays in the presence or absence of calcein. A dose–response curve with increasing doses of calcein from 10 µM to 500 µM was carried out with immunoprecipitated CDK6 (Fig. 1a), with an IC_{50} of 75 µM. Calcein at this concentration produced similar effects when CDK4, cyclin D1 or cyclin D3 were immunoprecipitated (Fig. 1b), but did not inhibit CDK1 or CDK2 kinase activities at any of the concentrations tested (Figure SM2.A supplementary material). As expected from *in silico* complex dynamics, the interaction of calcein with CDK6 seemed to be through the p16^{INK4a} binding site, as calcein was able to displace p16^{INK4a} from the immunoprecipitated enzyme (Figure SM2.B, supplementary material). These results demonstrate that calcein interacts selectively with CDK4 and CDK6 at the p16^{INK4a} binding site, inhibiting their kinase activity without affecting CDK2 and CDK1 activities.

To examine whether calcein penetrates the cell membrane and inhibits intracellular CDK4 and CDK6 activities, we used human colon adenocarcinoma HCT116 cells, as they have a silenced wild-type p16^{INK4A} gene and only express a mutant allele (Myohanen et al. 1998). Increasing doses of calcein in the media induced a progressive inhibition of HCT116 cell viability, presenting a rather high IC_{50} of 400 µM after 72 h of treatment. The calcein acetoxymethyl-ester (calcein AM) and *tert*-butoxy methyl ester (calcein tBM), which are more lipophilic and diffusible through the cytoplasmic membrane than the non-esterified calcein, induced a stronger inhibition of HCT116 cell viability, with IC_{50} values of 0.6 and 80 µM, respectively. Treatment of HCT116 cells with the non-esterified calcein or with calcein AM decreased the phosphorylation of the serine 780 of pRb, which is a specific target for CDK4 and CDK6 (Fig. 2a). In addition, calcein AM arrested the cell cycle in G_1 of synchronous HCT116 cells (Fig. 2b).

Journal : Large 11306 Dispatch : 27-6-2011 Pages : 11
Article No. : 328 LE TYPESET
MS Code : MEBO-474 CP DISK

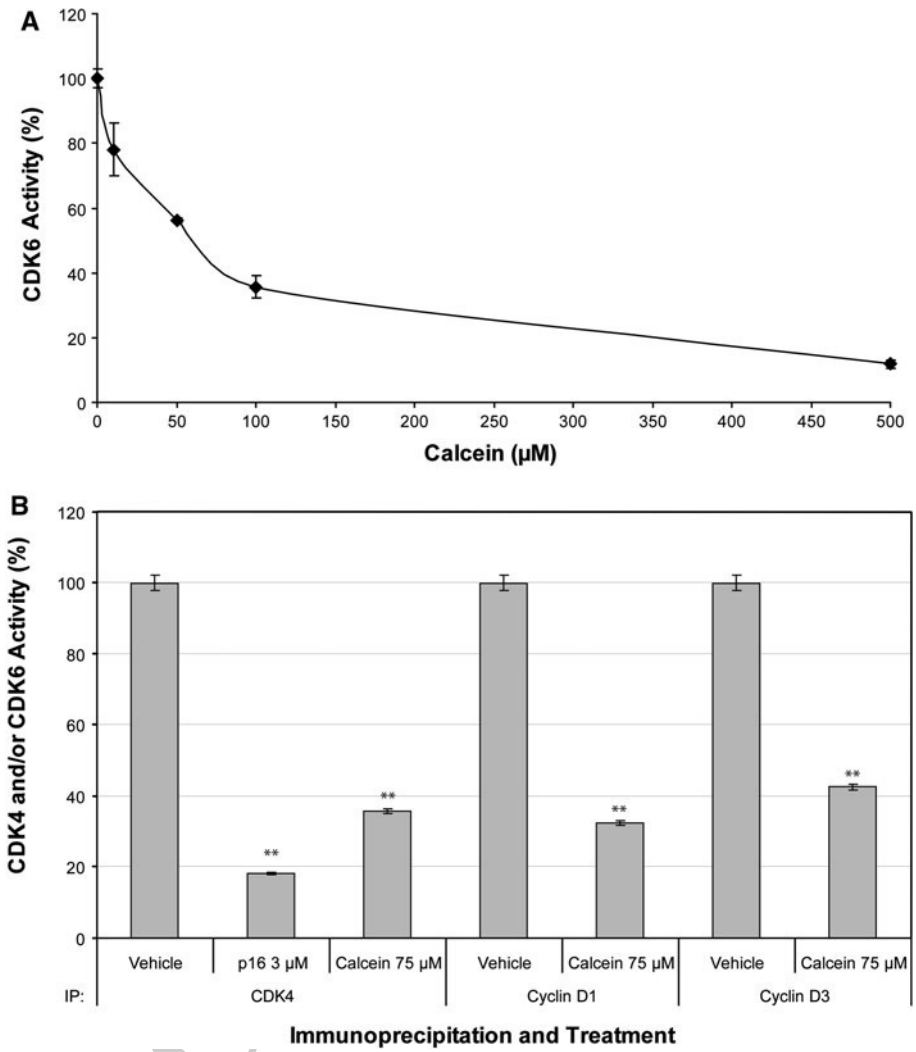

Fig. 1 Effect of calcein on kinase assays in inmunoprecipitated CDK6, CDK4, cyclin D1, and cyclin D3. **a** Dose–effect curve of non-esterified calcein on CDK6 activity (10–500 μM). **b** CDK4, cyclin D1 and cyclin D3 immunoprecipitations and kinase assays tested in the presence of 75 μM of non-esterified calcein and $p16^{INK4a}$ (3 μM). pGST-Rb (379–928) fusion protein was used as a substrate. Mean + SD; $n = 3$. (*) indicates $P < 0.05$ and (**) indicates $P < 0.01$ compared to vehicle

All these data suggest a molecular mechanism of action of calcein and its esters through the inhibition of CDK4 and CDK6, which in turn affects cell cycle regulation.

3.3 Metabolic effects caused by the inhibition of the CDKs responsible for G_1/S transition

HCT116 human colon adenocarcinoma cells exposed to increasing concentrations of calcein AM were incubated for 72 h with 10 mM glucose 50% enriched in [1,2-$^{13}C_2$]-D-glucose. The calcein AM concentrations were the IC_{25} (0.36 μM), IC_{50} (0.61 μM) and IC_{75} (1.0 μM) after 72 h of treatment. In parallel, we also performed incubations with immortalized mouse embryonic fibroblasts (Ct MEF) control and knockout for CDK4, CDK6 and CDK2 (TKO MEF) in the presence of the same tracer, to check whether the metabolic changes induced by calcein AM on HCT116 cells were characteristic of the inhibition of the CDKs responsible for the G_1/S transition. These MEF cell lines (Ct and TKO) constitute an additional new tool that could elucidate the effects of the permanent absence of these CDKs in vivo and their contributions to cell cycle progression and the robust tumor metabolic adaptation.

Lactate and ribose from RNA synthesized from the tracer [1,2-$^{13}C_2$]-D-glucose were measured using gas chromatography coupled to mass spectrometry (GC–MS). Table 1 shows the pondered values of the ^{13}C-enriched isotopologues, m1/Σm and m2/Σm, of lactate and ribose from RNA. The molar enrichment Σmn of ribose from RNA is also shown.

Lactate m2 isotopologues (lactate molecules that contain two ^{13}C atoms) originated from [1,2-$^{13}C_2$]-D-glucose converted to lactate through glycolysis, whereas lactate m1 isotopologues originated from the metabolization of the tracer through the oxidative step of the PPP and then recycled to glycolysis via the non-oxidative PPP. Calcein AM induced a dose–response decrease of m1/Σm and an increase of m2/Σm in HCT116 cells. This drop of m1/Σm suggests that calcein AM reduces the contribution of the oxidative PPP flux in lactate synthesis. Similarly, when

Journal : Large 11306 | Dispatch : 27-6-2011 | Pages : 11
Article No. : 328 | LE | TYPESET
MS Code : MEBO-474 | CP | DISK

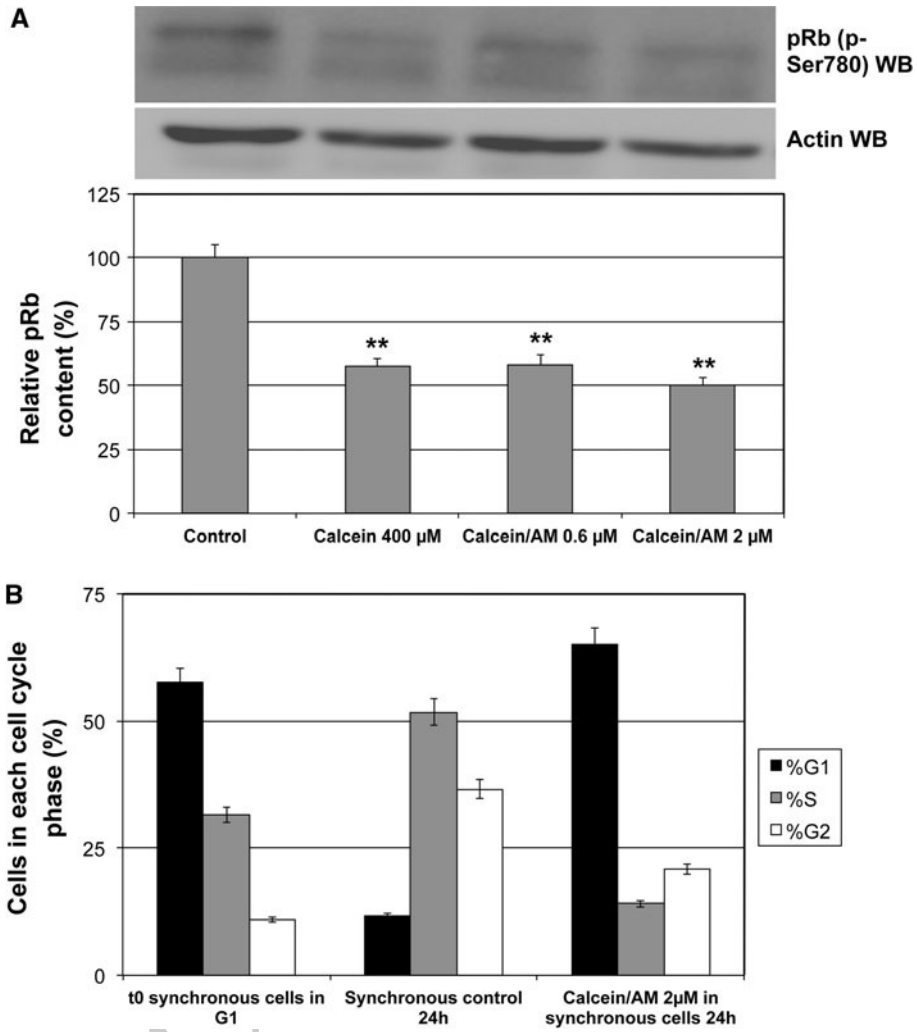

Fig. 2 Phosphorylation of serine780 of pRb and cell cycle analysis. **a** HCT116 cells were treated with 400 µM or with 0.6 and 2 µM of calcein AM for 24 h and the extracts were blotted specifically against phosphoserine 780 of pRb. **b** Synchronous HCT116 cells in the G_1 phase at time 0 h (t0 synchronous control) and after 24 h with or without treatment with calcein AM 2 µM. (*) indicates $P < 0.05$ and (**) indicates $P < 0.01$. Both experiments were performed three times (Mean + SD; $n = 3$). One representative example is shown in each case

Table 1 Isotopologue distribution in lactate and ribose. M1/Σm and m2/Σm were determined in lactate isolated from incubation medium and in ribose isolated from RNA. Σmn in ribose isolated from RNA was also measured

Isotopologue distribution analysis						
	HCT116				MEF	
Lactate	Ct	IC_{25}	IC_{50}	IC_{75}	Ct	TKO
m1/∑m	0.075 ± 0.003	0.075 ± 0.001	0.064 ± 0.003**	0.065 ± 0.002**	0.104 ± 0.000	0.070 ± 0.020*
m2/∑m	0.919 ± 0.003	0.918 ± 0.002	0.928 ± 0.002**	0.926 ± 0.002*	0.835 ± 0.049	0.843 ± 0.043
Ribose	Ct	IC_{25}	IC_{50}	IC_{75}	Ct	TKO
m1/∑m	0.544 ± 0.003	0.522 ± 0.002***	0.496 ± 0.003***	0.474 ± 0.003***	0.450 ± 0.002	0.414 ± 0.002***
m2/∑m	0.303 ± 0.000	0.324 ± 0.001***	0.343 ± 0.004***	0.364 ± 0.002***	0.385 ± 0.002	0.420 ± 0.002***
∑mn	0.839 ± 0.016	0.858 ± 0.030	0.811 ± 0.098**	0.668 ± 0.055*	0.754 ± 0.008	0.718 ± 0.008**

* $P < 0.05$; ** $P < 0.01$; *** $P < 0.001$. Experiments were performed twice. Results from one of them are shown (Mean + SD; $n = 3$)

MEF cell lines were incubated with [1,2-$^{13}C_2$]-D-glucose, the deletion of CDK4, CDK6 and CDK2 reduced m1/Σm lactate, indicating that TKO MEF cells had a reduced contribution of the oxidative pathway of PPP in lactate synthesis. Moreover, the pentose cycle activity decreased progressively in HCT116 cells treated with growing doses of calcein AM, and was 13.75% lower in the condition where the cells were treated with the calcein AM IC_{75} concentration (0.026 ± 0.001 in Ct vs. 0.023 ± 0.001 in IC_{75}). Similarly, pentose cycle activity in TKO MEF cells was 32.35% lower than in Ct MEF (0.040 ± 0.002 in Ct vs. 0.027 ± 0.008 in TKO). This decreased pentose cycle

Journal : Large 11306 | Dispatch : 27-6-2011 | Pages : 11
Article No. : 328 | LE | TYPESET
MS Code : MEBO-474 | CP | DISK

activity reinforced the hypothesis of a diminution of the oxidative PPP flux and a decrease in its contribution to glucose metabolism when the G_1/S-phase of the cell cycle is perturbed.

Calcein AM treatment in HCT116 cells also resulted in a slight decrease in the incorporation of ^{13}C atoms from glucose into nucleic acid ribose (Table 1). The average number of ^{13}C atoms per ribose molecule (Σmn) was reduced by 20% at the dose of IC_{75} of calcein AM in HCT116 cells. As suggested by the above-described decrease in lactate m1/Σm data, the reduction of ribose synthesis in HCT116 cells could be caused by reduced substrate flux through the oxidative steps of the PPP. Furthermore, calcein AM treatment in HCT116 cells caused a dose-dependent m1/Σm decrease as well as a linear increase of m2/Σm ribose (Table 1). This was in accordance with the results obtained in lactate measurements and denoted a clear attenuation of the flux through the oxidative PPP.

Furthermore, TKO MEFs had a lower proliferation rate than Ct MEFs (Ct MEF: 0.26 h^{-1} vs. TKO MEF: 0.12 h^{-1}), the total label incorporation in ribose (Σmn) being lower than that of Ct MEFs (Table 1). Moreover, deletion of CDK4, CDK6 and CDK2 resulted in a decrease in the percentage of ribose m1/Σm and an increase in ribose m2/Σm, which suggests a decrease in the use of the oxidative branch of the PPP. This was in accordance with the results obtained in lactate measurements and denoted a clear attenuation of the flux through the oxidative PPP. Similarly, the oxidative/non-oxidative ratio of PPP was 14% lower for TKO MEFs than for Ct MEFs (0.78 ± 0.00 and 0.91 ± 0.01, respectively). Equally, all calcein AM treatments showed a lower oxidative/non-oxidative ratio of PPP compared to the control treatments (8.42, 18, and 31.90% lower for the IC_{25}, IC_{50}, and IC_{75} treated HCT116, respectively, 1.27 ± 0.00 being for control HCT116 cells). It has been reported that this ratio is higher in tumor cells compared to normal cells (Ramos-Montoya et al. 2006).

To provide information on the relative importance of the two pathways of pentose phosphate production for the viability of the cell, we used phenotype phase-plane analysis. Phenotype phase-plane analysis is the analysis of substrate production and utilization of cells and is an important aspect of reaction network analysis (Edwards et al. 2002; Lee 2006). Figure 3 contains the phase-plane analysis of the normalized ribose isotopologues m1 and m2, where values for oxidative ribose synthesis are plotted against non-oxidative ribose synthesis. The line of optimality is arbitrarily defined as the line drawn through the point for the basal state (Ct Control treatment or Ct MEF) corresponding to conditions satisfying the optimal conditions for growth (objective function). The slope of the line represents the optimal ratio of ribose formed through the oxidative pentose phosphate pathway to a given level of non-oxidative ribose synthesis for the tumor cells. When a line is drawn from a phenotype (a point on the phase-plane), parallel to the major axis, the intersection between the line of optimality and the parallel line indicates the degree of optimality relative to the basal state. Using metabolic phenotype phase-plane analysis, we saw that increasing doses of calcein AM or the deletion of the main CDKs of the G_1/S-phase transition resulted in a more dramatic imbalance between oxidative/non-oxidative PPP.

According to these data, the representation of m1/Σm *vs* m2/Σm in a phenotype phase-plane analysis confirmed the same tendency as in calcein AM-treated cells: the deletion of the CDKs, which phosphorylate pRb, caused an imbalance of the PPP towards the non-oxidative branch (Fig. 3).

3.4 Sugar phosphate pool decreases when cell cycle does not progress

Changes in the absolute concentrations of the intermediary sugar phosphates reflect variations in the metabolic flux profile distribution. Pentose phosphate, triose phosphate and hexose phosphate pools were quantified in HCT116 cells treated with IC_{50} of calcein AM (0.6 μM) and control

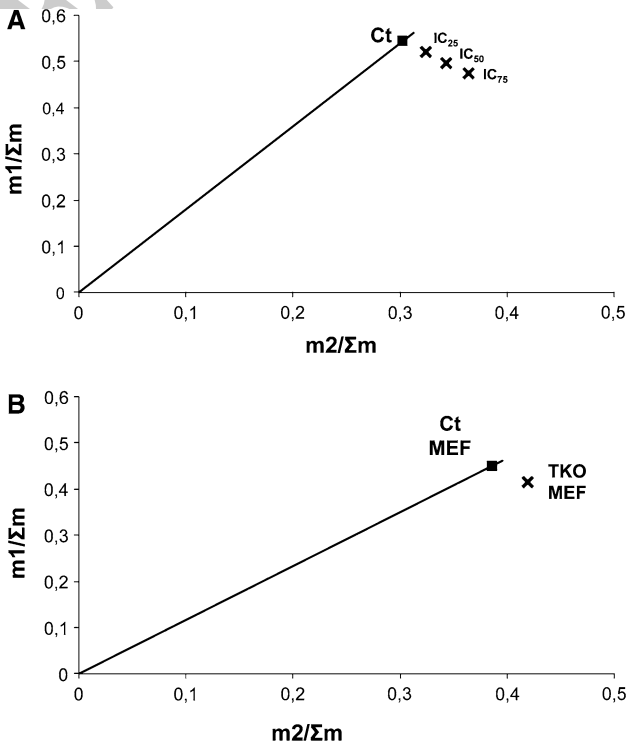

Fig. 3 ^{13}C ribose label distribution. Phase-plane analysis of the normalized ribose isotopologues m1 and m2. **a** HCT116 cells treated without (Ct) or with IC_{25}, IC_{50}, and IC_{75} doses of calcein AM; and **b** the control mouse embryonic fibroblasts (Ct MEF) and the MEF knockout for CDK4, CDK6, and CDK2 (TKO MEF)

Journal : Large 11306 Dispatch : 27-6-2011 Pages : 11
Article No. : 328 LE TYPESET
MS Code : MEBO-474 CP DISK

and TKO MEFs (data not shown). Inhibition of CDK4 and CDK6 function using a calcein AM inhibitor or the knockout cell model resulted in decrease in the concentration of fructose-1,6-*bis*phosphate, pentose and triose phosphate intermediaries. Although, these changes were not significant, they showed a tendency in which the arrest in the G_1 phase of the cell cycle alters the profile of sugar phosphate concentrations.

4 Discussion

Evidence indicates that CDK4 and CDK6 are excellent targets for the design of new anti-tumor drugs (Landis et al. 2006; Yu et al. 2006; Malumbres and Barbacid 2006; Marzec et al. 2006). However, the design of good specific inhibitors against the activity of these kinases has not been successful until now. Different strategies have been employed in the search for good inhibitors but almost none of them have been successful due to their unspecificity and the subsequent side effects (Fry et al. 2004; McInnes 2008; Menu et al. 2008). Thus, there is emerging interest in developing new strategies to search for selective inhibitors of CDK4 and CDK6 for cancer chemotherapy (Mahale et al. 2006). To this end, in this study we used a new set of bioinformatic tools to design CDK4 and CDK6 inhibitors that mimic their natural inhibitor $p16^{INK4a}$. One of these inhibitors was calcein.

Calcein AM is a fluorescent dye that localizes intracellularly after esterase-dependent cellular trapping and has shown cytotoxic activity against various established human tumor cell lines at relatively low concentrations (Jonsson et al. 1996; Liminga et al. 2000). Furthermore, Liminga and collaborators found that calcein AM caused a strong apoptotic response within hours of exposure and tested it on a panel of ten different cell lines, but they failed to find its precise mechanism of action to inhibit cell proliferation (Liminga et al. 1999; Liminga et al. 2000; Liminga et al. 1995). According to our results, calcein carboxylic esters easily penetrate HCT116 cells, inhibiting cell viability at relatively low doses compared with the non-esterified calcein. We have also shown that calcein (the active form inside the cell of the calcein AM ester) specifically inhibited CDK4 and CDK6 (cyclin D-related activities), inducing inhibition of pRb phosphorylation, which is required for entering the S-phase of the cell cycle (Lundberg and Weinberg 1998; Malumbres et al. 2004). The potential of calcein to avoid the entrance of treated cells into the S-phase was further validated here, as calcein AM treatment on HCT116 cells provoked a strong G_1-phase cell cycle arrest.

Having elucidated the effects of calcein on the cell cycle, we proceeded to characterize in depth the effects of inhibiting CDK4 and CDK6 activities on the metabolic profile of the HCT116 cells. We have previously demonstrated that the balance between oxidative and non-oxidative branches of the PPP is essential to maintain proliferation in cancer cells and is a vulnerable target within the cancer metabolic network for potential new therapies for overcoming drug resistance (Ramos-Montoya et al. 2006). Our results here show that increasingly high calcein AM concentrations result in a stronger imbalance of PPP in favor of the non-oxidative branch (Fig. 4). Using metabolic phenotype phase-plane analysis, we deduced that the most efficient doses of calcein AM in the inhibition of tumor cell growth result in a more dramatic imbalance between oxidative and non-oxidative branches of PPP. The perturbation of this imbalance results in a state of metabolic inefficiency and consequently could lead to a pause in cell proliferation or even cell apoptosis. To ensure that the metabolic alterations induced by calcein AM in HCT116 cells were due to the specific inhibition of CDK4 and CDK6 activities induced by this compound, we also characterized the metabolic profile of control (Ct) and triple knockout (TKO) MEFs. These results showed that the lack of functionality of CDK4, CDK6 and CDK2 induced changes in the metabolic profile of fibroblasts that correlate with the alterations induced by calcein AM in the metabolic profile of HCT116 tumor cells. These results support our hypothesis that inhibition of CDK4 and CDK6 was responsible for the oxidative/non-oxidative imbalance in PPP induced by calcein AM.

We recently reported a specific increase in the activities of two key enzymes of PPP, glucose-6-phosphate dehydrogenase for the oxidative branch and transketolase for the non-oxidative branch, during the S/G_2 phases of the cell cycle, in particular during the S-phase, when the synthesis of nucleotides is required. Such an increase in the PPP enzyme

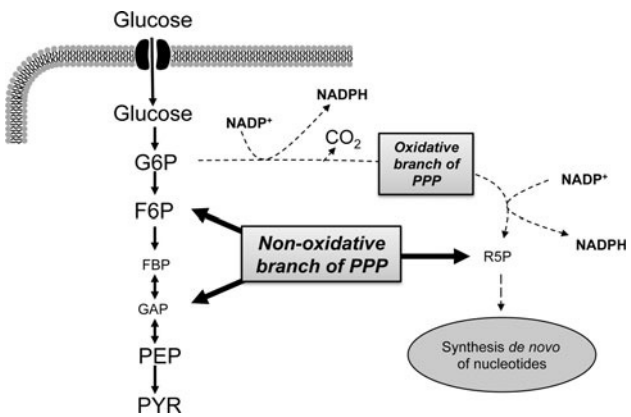

Fig. 4 Metabolic changes associated to CDK4/6 inhibition. CDK4 and CDK6 inhibition leads to an imbalance between the oxidative and non-oxidative branches of the pentose phosphate pathway towards the non-oxidative branch. *Thick lines* indicate enhanced metabolic routes. *Dotted lines* indicate less active metabolic routes and *smaller font sizes* indicate lower intermediate concentrations

Journal : Large 11306 Dispatch : 27-6-2011 Pages : 11
Article No. : 328 LE TYPESET
MS Code : MEBO-474 CP DISK

activities correlates with a relative increase in the pentose phosphate pool and a progressive increase in the balance between oxidative and non-oxidative branches of PPP in the S and G_2 phases (Vizan et al. 2009). This means that the contribution of the oxidative branch to ribose-5-phosphate synthesis is relatively increased when the cycle progresses through the S-phase (Vizan et al. 2009). In this article, the results support this assertion, showing a decrease in this balance when HCT116 cells were treated with calcein AM or when fibroblasts did not express functional CDK4, CDK6, and CDK2 and their progress through the cell cycle was compromised. Moreover, ^{13}C incorporation from glucose into RNA ribose was lower both in HCT116 treated with calcein AM and in TKO MEFs, indicating that ribose-5-phosphate synthesis decreases when the entrance of the cell into the S-phase is inhibited. Additionally, in this work we have shown that the imbalance in PPP induced by the inhibition of CDK4 and CDK6 is able to slightly compromise the balance in the overall central carbon metabolic network of the cell, which is reflected in a non-significant change in the levels of intermediary sugar phosphates (Fig. 4). The results presented in this paper regarding the metabolic consequences of the inhibition of CDK4 and CDK6 highlights the metabolic requirements of the cell cycle and points to CDK4 and CDK6 as interesting drug targets to be explored in a wider range of cancer types.

5 Concluding remarks

The forced imbalance of the PPP towards the oxidative branch is a possible Achilles' heel in the robust tumor metabolic adaptation. It has been shown that effective anti-tumor strategies against this target can be designed not only with drugs that force this imbalance even further (Ramos-Montoya et al. 2006), but also using drugs that recover the oxidative/non-oxidative balance in the non-tumor cells. The data presented here demonstrate that the inhibition of CDK4 and CDK6 using calcein AM not only inhibits the progression of the cell cycle, but also disrupts this oxidative/non-oxidative imbalance of PPP, which has been described as essential for tumor proliferation, reinforcing the interest of CDK4 and CDK6 as targets in cancer therapy.

Furthermore, we suggest that calcein could be a key factor in the development of a new family of selective cyclin D-dependent kinases inhibitors based on its structure. The improved understanding of the specific effects of the inhibition of CDK4 and CDK6 on tumor cell central metabolic networks shown in this paper opens up new avenues for the design of combination therapies with drugs that directly inhibit those pathways and also to the use of specific CDK4 and CDK6 inhibitors to impair metabolic adaptations that support tumor cell cycle progression.

Acknowledgments The authors thank Mrs Ursula Valls for her technical support in the experiments and Dr David Santamaria for his help in MEF procedures. MEF cells were a generous gift from Dr Mariano Barbacid, CNIO-Madrid (Spain). This study was supported by the projects SAF2008-00164 and RD06/0020/0046 (to MC), RD06/0020/0010 (to OB) and SAF2007-60491 (by NA) funded by the Ministerio de Ciencia e Innovación-Spanish government and European Union FEDER funds. It has also received financial support from the European Union-funded project ETHERPATHS (FP7-KBBE-222639) (http://www.etherpaths.org/) and from the Agència de Gestió d'Ajuts Universitaris i de Recerca (AGAUR)-Generalitat de Catalunya (2005SGR00204 and predoctoral fellowship of M.Z). MC acknowledges the support received through the prize "ICREA Academia" for excellence in research, funded by ICREA foundation-Generalitat de Catalunya.

References

Boros, L. G., Puigjaner, J., Cascante, M., Lee, W. N., Brandes, J. L., Bassilian, S., et al. (1997). Oxythiamine and dehydroepiandrosterone inhibit the nonoxidative synthesis of ribose and tumor cell proliferation. *Cancer Research, 57*, 4242–4248.

Bradford, M. M. (1976). A rapid and sensitive method for the quantitation of microgram quantities of protein utilizing the principle of protein-dye binding. *Analytical Biochemistry, 72*, 248–254.

Comin-Anduix, B., Boros, L. G., Marin, S., Boren, J., Callol-Massot, C., Centelles, J. J., et al. (2002). Fermented wheat germ extract inhibits glycolysis/pentose cycle enzymes and induces apoptosis through poly(ADP-ribose) polymerase activation in Jurkat T-cell leukemia tumor cells. *Journal of Biological Chemistry, 277*, 46408–46414.

Edwards, J. S., Ramakrishna, R., & Palsson, B. O. (2002). Characterizing the metabolic phenotype: a phenotype phase plane analysis. *Biotechnology and Bioengineering, 77*, 27–36.

Frangioni, J. V., & Neel, B. G. (1993). Solubilization and purification of enzymatically active glutathione S-transferase (pGEX) fusion proteins. *Analytical Biochemistry, 210*, 179–187.

Fry, D. W., Harvey, P. J., Keller, P. R., Elliott, W. L., Meade, M., Trachet, E., et al. (2004). Specific inhibition of cyclin-dependent kinase 4/6 by PD 0332991 and associated antitumor activity in human tumor xenografts. *Molecular Cancer Therapeutics, 3*, 1427–1438.

Graf, F., Koehler, L., Kniess, T., Wuest, F., Mosch, B., & Pietzsch, J. (2009). Cell cycle regulating kinase Cdk4 as a potential target for tumor cell treatment and tumor imaging. *Journal of Oncology, 2009*, 106378.

Hall, M., & Peters, G. (1996). Genetic alterations of cyclins, cyclin-dependent kinases, and Cdk inhibitors in human cancer. *Advances in Cancer Research, 68*, 67–108.

Harlow, E. & Lane, D. (Eds.). (1988). Antibodies: a laboratory manual (p. 469). New York: Cold Spring Harbor Laboratory Press.

Jonsson, B., Liminga, G., Csoka, K., Fridborg, H., Dhar, S., Nygren, P., et al. (1996). Cytotoxic activity of calcein acetoxymethyl ester (calcein/AM) on primary cultures of human haematological and solid tumours. *European Journal of Cancer, 32A*, 883–887.

Kuo, W., Lin, J., & Tang, T. K. (2000). Human glucose-6-phosphate dehydrogenase (G6PD) gene transforms NIH 3T3 cells and

Journal : Large 11306 | Dispatch : 27-6-2011 | Pages : 11
Article No. : 328 | ☐ LE | ☐ TYPESET
MS Code : MEBO-474 | ☑ CP | ☑ DISK

induces tumors in nude mice. *International Journal of Cancer, 85*, 857–864.

Laemmli, U. K. (1970). Cleavage of structural proteins during the assembly of the head of bacteriophage T4. *Nature, 227*, 680–685.

Landis, M. W., Pawlyk, B. S., Li, T., Sicinski, P., & Hinds, P. W. (2006). Cyclin D1-dependent kinase activity in murine development and mammary tumorigenesis. *Cancer Cell, 9*, 13–22.

Lee, W. N. P. (2006). Characterizing phenotype with tracer based metabolomics. *Metabolomics, 2*, 31–39.

Lee, W. N., Boros, L. G., Puigjaner, J., Bassilian, S., Lim, S., & Cascante, M. (1998). Mass isotopomer study of the nonoxidative pathways of the pentose cycle with [1,2–13C2]glucose. *American Journal of Physiology, 274*, E843–E851.

Lee, W. N., Byerley, L. O., Bergner, E. A., & Edmond, J. (1991). Mass isotopomer analysis: theoretical and practical considerations. *Biological Mass Spectrometry, 20*, 451–458.

Liminga, G., Jonsson, B., Nygren, P., & Larsson, R. (1999). On the mechanism underlying calcein-induced cytotoxicity. *European Journal of Pharmacology, 383*, 321–329.

Liminga, G., Martinsson, P., Jonsson, B., Nygren, P., & Larsson, R. (2000). Apoptosis induced by calcein acetoxymethyl ester in the human histiocytic lymphoma cell line U-937 GTB. *Biochemical Pharmacology, 60*, 1751–1759.

Liminga, G., Nygren, P., Dhar, S., Nilsson, K., & Larsson, R. (1995). Cytotoxic effect of calcein acetoxymethyl ester on human tumor cell lines: drug delivery by intracellular trapping. *Anticancer Drugs, 6*, 578–585.

Lundberg, A. S., & Weinberg, R. A. (1998). Functional inactivation of the retinoblastoma protein requires sequential modification by at least two distinct cyclin-cdk complexes. *Molecular and Cellular Biology, 18*, 753–761.

Mahale, S., Aubry, C., Jenkins, P. R., Marechal, J. D., Sutcliffe, M. J., & Chaudhuri, B. (2006). Inhibition of cancer cell growth by cyclin dependent kinase 4 inhibitors synthesized based on the structure of fascaplysin. *Bioorganic Chemistry, 34*(5), 287–297.

Malumbres, M., & Barbacid, M. (2001). To cycle or not to cycle: a critical decision in cancer. *Nature Reviews Cancer, 1*, 222–231.

Malumbres, M., & Barbacid, M. (2006). Is cyclin D1-CDK4 kinase a bona fide cancer target? *Cancer Cell, 9*, 2–4.

Malumbres, M., Sotillo, R., Santamaria, D., Galan, J., Cerezo, A., Ortega, S., et al. (2004). Mammalian cells cycle without the D-type cyclin-dependent kinases Cdk4 and Cdk6. *Cell, 118*, 493–504.

Marzec, M., Kasprzycka, M., Lai, R., Gladden, A. B., Wlodarski, P., Tomczak, E., et al. (2006). Mantle cell lymphoma cells express predominantly cyclin D1a isoform and are highly sensitive to selective inhibition of CDK4 kinase activity. *Blood, 108*, 1744–1750.

Matito, C., Mastorakou, F., Centelles, J. J., Torres, J. L., & Cascante, M. (2003). Antiproliferative effect of antioxidant polyphenols from grape in murine Hepa-1c1c7. *European Journal of Nutrition, 42*, 43–49.

McInnes, C. (2008). Progress in the evaluation of CDK inhibitors as anti-tumor agents. *Drug Discovery Today, 13*, 875–881.

Menu, E., Garcia, J., Huang, X., Di Liberto, M., Toogood, P. L., Chen, I., et al. (2008). A novel therapeutic combination using PD 0332991 and bortezomib: study in the 5T33MM myeloma model. *Cancer Research, 68*, 5519–5523.

Mosmann, T. (1983). Rapid colorimetric assay for cellular growth and survival: application to proliferation and cytotoxicity assays. *Journal of Immunological Methods, 65*, 55–63.

Myohanen, S. K., Baylin, S. B., & Herman, J. G. (1998). Hypermethylation can selectively silence individual p16ink4A alleles in neoplasia. *Cancer Research, 58*, 591–593.

Poulsen, H. S., & Frederiksen, P. (1981). Glucose-6-phosphate dehydrogenase activity in human breast cancer. Lack of association with oestrogen receptor content. *Acta Pathol Microbiol Scand [A], 89*, 263–270.

Ramos-Montoya, A., Lee, W.-N. P., Bassilian, S., Lim, S., Trebukhina, R. V., Kazhyna, M. V., et al. (2006). Pentose phosphate cycle oxidative and non-oxidative balance: a new vulnerable target for overcoming drug resistance in cancer. *International Journal of Cancer, 119*, 2733–2741.

Rubio-Martinez, J., Pinto, M., Tomas M.S., Perez, J. J. (2005). Dock_Dyn: a program for fast molecular docking using molecular dynamics information. University of Barcelona and Technical University of Catalonia.

Santamaria, D., & Ortega, S. (2006). Cyclins and CDKS in development and cancer: lessons from genetically modified mice. *Frontiers in Bioscience, 11*, 1164–1188.

Shapiro, G. I. (2006). Cyclin-dependent kinase pathways as targets for cancer treatment. *Journal of Clinical Oncology, 24*, 1770–1783.

Sherr, C. J. (1996). Cancer cell cycles. *Science, 274*, 1672–1677.

Sherr, C. J., & Roberts, J. M. (2004). Living with or without cyclins and cyclin-dependent kinases. *Genes and Development, 18*, 2699–2711.

Smith, D. B., & Johnson, K. S. (1988). Single-step purification of polypeptides expressed in *Escherichia coli* as fusions with glutathione S-transferase. *Gene, 67*, 31–40.

Villacanas, O., Perez, J. J., & Rubio-Martinez, J. (2002). Structural analysis of the inhibition of Cdk4 and Cdk6 by p16(INK4a) through molecular dynamics simulations. *Journal of Biomolecular Structure and Dynamics, 20*, 347–358.

Villacanas, O., & Rubio-Martinez, J. (2006). Reducing CDK4/6–p16(INK4a) interface. Computational alanine scanning of a peptide bound to CDK6 protein. *Proteins, 63*, 797–810.

Vizan, P., Alcarraz-Vizán, G., Diaz-Moralli, S., Rodriguez-Prados, J. C., Zanuy, M., Centelles, J. J., et al. (2007). Quantification of intracellular phosphorylated carbohydrates in HT29 human colon adenocarcinoma cell line using liquid chromatography-electrospray ionization tandem mass spectrometry. *Analytical Chemistry, 79*(13), 5000–5005.

Vizan, P., Alcarraz-Vizan, G., Diaz-Moralli, S., Solovjeva, O. N., Frederiks, W. M., & Cascante, M. (2009). Modulation of pentose phosphate pathway during cell cycle progression in human colon adenocarcinoma cell line HT29. *International Journal of Cancer, 124*, 2789–2796.

Vizán, P., Mazurek, S., & Cascante, M. (2008). Robust metabolic adaptation underlying tumor progression. *Metabolomics, 4*, 1–12.

Warburg, O. (1956). Origin of cancer cells. *Oncologia, 9*, 75–83.

Yu, Q., Sicinska, E., Geng, Y., Ahnstrom, M., Zagozdzon, A., Kong, Y., et al. (2006). Requirement for CDK4 kinase function in breast cancer. *Cancer Cell, 9*, 23–32.

Journal : Large 11306 | Dispatch : 27-6-2011 | Pages : 11
Article No. : 328 | ☐ LE | ☐ TYPESET
MS Code : MEBO-474 | ☑ CP | ☑ DISK